

# Heat flux across an open pore enables the continuous replication and selection of oligonucleotides towards increasing length

Moritz Kreising<sup>‡</sup>, Lorenz Keil<sup>‡</sup>, Simon Lanzmich<sup>‡</sup> and Dieter Braun<sup>\*</sup>

**The replication of nucleic acids is central to the origin of life. On the early Earth, suitable non-equilibrium boundary conditions would have been required to surmount the effects of thermodynamic equilibrium such as the dilution and degradation of oligonucleotides. One particularly intractable experimental finding is that short genetic polymers replicate faster and outcompete longer ones, which leads to ever shorter sequences and the loss of genetic information. Here we show that a heat flux across an open pore in submerged rock concentrates replicating oligonucleotides from a constant feeding flow and selects for longer strands. Our experiments utilize the interplay of molecular thermophoresis and laminar convection, the latter driving strand separation and exponential replication. Strands of 75 nucleotides survive whereas strands half as long die out, which inverts the above dilemma of the survival of the shortest. The combined feeding, thermal cycling and positive length selection opens the door for a stable molecular evolution in the long-term microhabitat of heated porous rock.**

From a wide range of exploratory experiments much is known about the capabilities and limitations of chemical replication systems<sup>1–6</sup>. It has become increasingly clear that such replicators are delicate systems that require a suitable supportive microenvironment to host non-equilibrium conditions. These conditions permit the sustainment of molecular evolution and the synthesis of molecules against equilibrating forces<sup>1,7–9</sup>. To the same end, modern cells provide active compartments of reduced entropy that protect genetic information against its thermodynamically favoured decay<sup>8,10</sup>. This is facilitated by sophisticated membrane-trafficking machinery and a metabolism that feeds on chemical low-entropy sources or light energy (Fig. 1a).

It has been known since Spiegelman's experiments in the late 1960s<sup>11</sup> that, even if humans assist with the assembly of an extracellular evolution system, genetic information from long nucleic acids is quickly lost. This is because shorter nucleic acids are replicated with faster kinetics and outcompete longer sequences. If mutations in the replication process can change the sequence length, the result is an evolutionary race towards ever shorter sequences.

In the experiments described here we present a counterexample. We demonstrate that heat dissipation across an open rock pore, a common setting on the early Earth<sup>12</sup> (Fig. 1b), provides a promising non-equilibrium habitat for the autonomous feeding, replication and positive length selection of genetic polymers. Previously, it has been argued that a temperature gradient spanning a submillimetre wide, closed compartment is able to accumulate dilute nucleotides, to enforce their polymerization or to concentrate lipids to form vesicles<sup>13–15</sup>.

Here we extend the concept to the geologically realistic case of an open pore with a slow flow passing through it. We find continuous, localized replication of DNA together with an inherent nonlinear selection for long strands. With an added mutation process, the shown system bodes well for an autonomous Darwinian evolution

based on chemical replicators with a built-in selection for increasing the sequence length. The complex interplay of thermal and fluid dynamic effects, which leads to a length-selective replication (Fig. 1c, (1)–(4)), is introduced in a stepwise manner.

## Results

**Accumulation.** The accumulation mechanism responsible for counterbalancing the mixing entropy relies on the interplay of thermophoresis and gravitationally driven convection (Fig. 2a and Supplementary Movie 1). In the presence of a temperature difference, thermophoresis drives the molecules horizontally from the warm left side to the cold right side. On a similar timescale, the fluid moves vertically by convection and carries the molecules with it. Convection deflects the horizontal thermophoretic depletion and amplifies it to give a strong vertical molecule accumulation<sup>16,17</sup> (see Methods). This interplay of molecular movement and fluid flow therefore results in an efficient net transport of oligonucleotides to the bottom of the compartment; the experiment is visualized in Fig. 2b (also see Supplementary Movie 2).

For oligonucleotides with a length of 75 bases, concentrations increase by a factor of ten per millimetre pore length, which results in a millionfold concentration increase for a 6 mm high pore. Larger nucleic acids are exponentially better trapped because their higher charge contributes quadratically to the achievable accumulation<sup>18,19</sup>. This length-selective accumulation bias can be directly detected experimentally (Supplementary Fig. 3). The accumulation counterbalances diffusional dilution and offers a solution to the concentration problem associated with the origin of life.

**Size-selective trapping from feeding flow.** To establish efficient feeding with replication-relevant monomers, we opened the pore at both ends. This permitted an upwards feeding flow through the pore that originated from the overall large-scale upwards flow in a hydrothermal situation. Interestingly, this led to all-or-nothing

Systems Biophysics, Physics Department, Center for Nanoscience, Ludwig-Maximilians-Universität München, 80799 Munich, Germany. <sup>†</sup>Present address: Max Planck Institute of Molecular Cell Biology and Genetics, 01307 Dresden, Germany. <sup>‡</sup>These authors contributed equally to this work.

\*e-mail: dieter.braun@physik.lmu.de

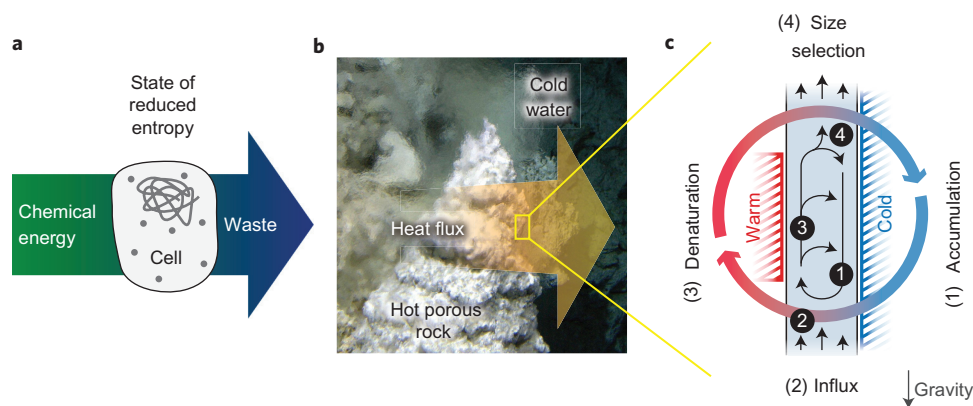


**Figure 1 | Reduction of local entropy is key for living systems and can be caused by the flux of thermal energy.** **a**, Modern cells feed on chemical energy, which enables them to host, maintain and replicate information-coding polymers, processes necessary for Darwinian evolution. **b**, The flux of thermal energy across geological cracks near a heat source (the white smoker<sup>28</sup> is adapted from an image courtesy of Deborah S. Kelley). **c**, (1) A thermal gradient across a millimetre-sized crack induces the accumulation of molecules by thermophoresis and convection. (2) A global throughflow imports nutrients into the open pore. (3) Exponential replication is facilitated by the local convection, which shuttles the molecules repetitively between warm and cold, and thus induces the cyclic denaturation of nucleotides. (4) The combination of influx, thermophoresis and convection selectively traps long molecules and flushes out short ones. The inflow speed determines the cut-off size of the resulting length selection. Mechanisms (1) to (4) are described in detail in this article.

trapping characteristics that depend on the strand length. We loaded an oligonucleotide ladder (20–200 base pairs (bp) dsDNA) in a 3.5 mm high and 70  $\mu\text{m}$  wide pore and introduced an upwards flow with a velocity of  $6\ \mu\text{m s}^{-1}$ . Using gel electrophoresis, we observed that nucleic acids above a certain threshold length were trapped inside the pore, whereas shorter

strands followed the upwards flow and were washed out of the pore (Fig. 3a and Supplementary Movie 3).

For a given velocity, this sharp length fractionation had a transition between 80 and 100 bp and can be understood by the interaction of the flow profile inside the trap with the thermophoretic concentration profile. The upwards feeding flow superimposes on the internal convection pattern, which generates an asymmetrical flow profile inside the trap (Fig. 3b). Long strands are pushed by thermophoresis into the descending flow at the cold side, transporting the molecules downwards. These are then localized against the upwards feeding flow at the bottom end of the heated section. Shorter strands experience weaker thermophoresis and the overall upwards flow drags them out of the trap.

The flow rate at which the solute nucleic acids start to move upwards and leave the pore depends monotonically on the strand length. Consequently, a gradual increase of the flow rate with time results in the sequential release of longer strands (Fig. 3c). The existence of the observed threshold length might come as a surprise, but a finite-element model that combines flow, diffusion and thermophoresis reproduces the behaviour of the trap in detail (Fig. 3d and Methods).

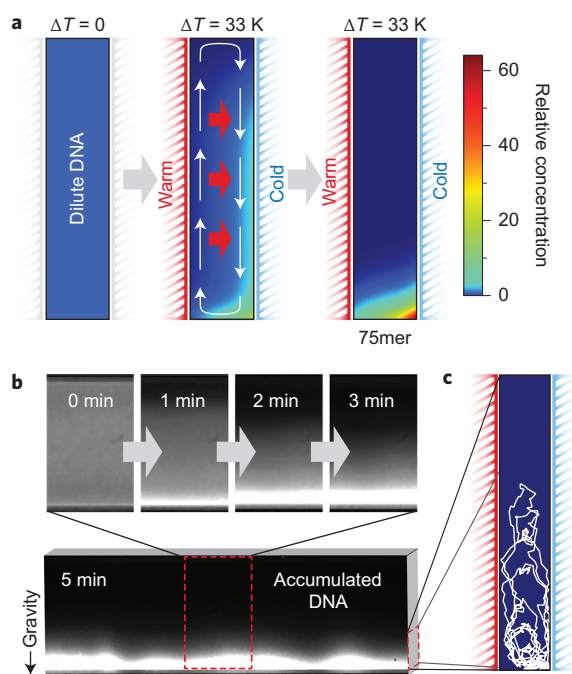


**Figure 2 | Accumulation of oligonucleotides.** **a**, The temperature gradient drives oligonucleotides horizontally from warm to cold by thermophoresis and simultaneously triggers the vertical thermal convection of water. Its combination results in a length-dependent accumulation at the bottom of an elongated pore within minutes (see Supplementary Movie 2). **b**, The accumulation of dilute double-stranded oligonucleotides (100–1,000mer) at the bottom is monitored within a 100  $\mu\text{m}$  thin and 2 mm high capillary via SYBR Green I fluorescence. **c**, The accumulation is dynamic: the nucleotides cycle between the warm and cold sides, visualized in white for a single 500mer of DNA.

**Exponential replication by convective thermal cycling.** Besides continuous feeding and length-selective trapping, the asymmetrically heated pore offers another important feature relevant to the origin of life: laminar convective temperature cycling of the accumulated nucleic acids<sup>20,21</sup>. This opens the door to Watson–Crick-type replication mechanisms, which are otherwise hindered by the considerable energy costs required to separate double-stranded oligonucleotides<sup>22</sup>. The thermal cycling can be predicted from a fluid dynamics model that includes thermophoresis and diffusion (Fig. 4a). It is sufficient to separate cyclically double-stranded DNA (dsDNA) to drive exponential base-by-base replication with duplication times on the order of minutes, as documented by SYBR Green I fluorescence (Fig. 4b and Supplementary Movie 4). Our focus was to study the boundary conditions that enable early chemical systems for oligonucleotide replication. For this, we chose the polymerase chain reaction (PCR) as a fast and well-characterized placeholder for the large family of template-directed replication mechanisms that depend on temperature oscillations for long substrates<sup>2–6</sup>.

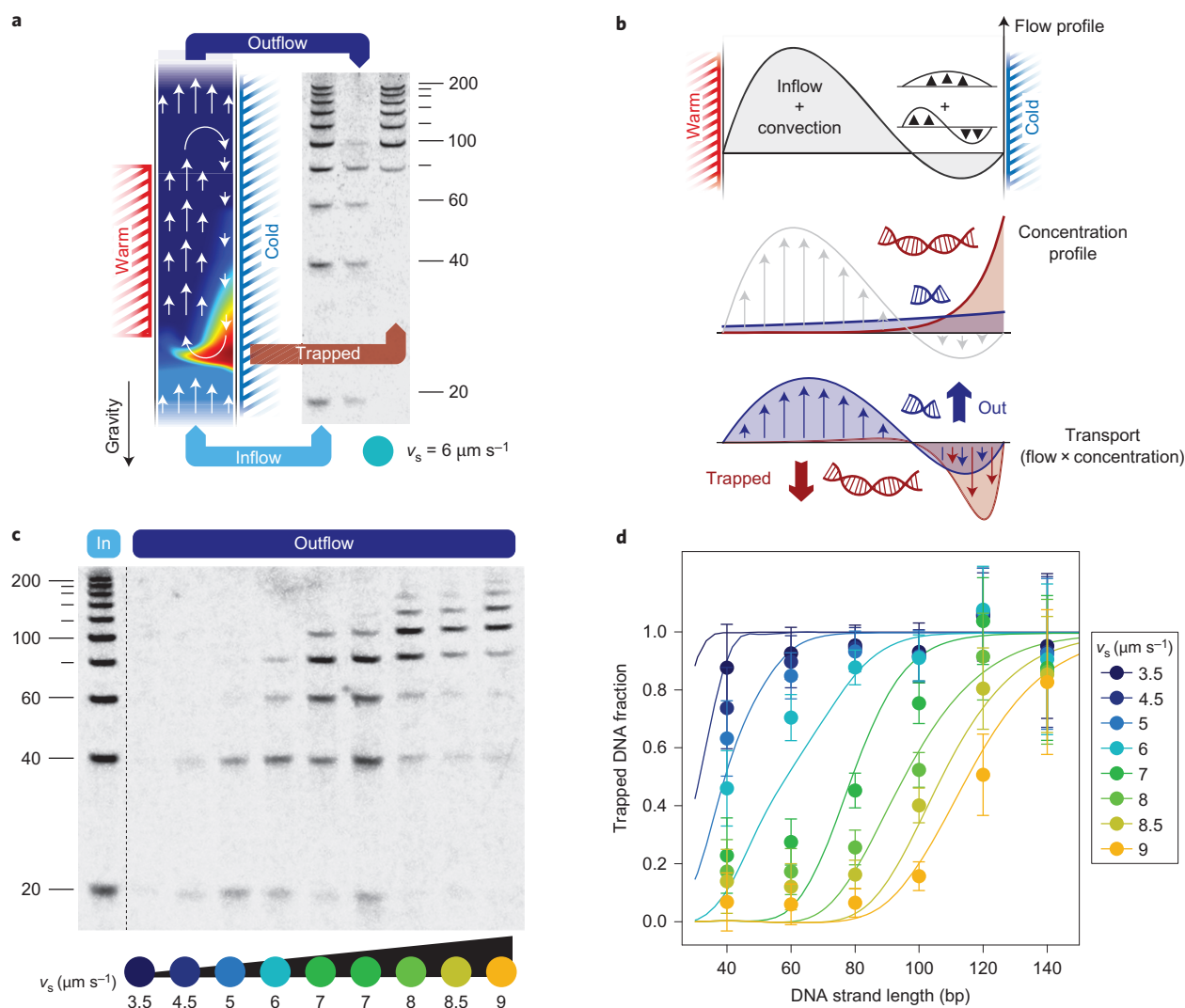


**Figure 3 | Heat-driven filter selecting for strand length.** **a**, A steady upwards feeding flow is triggered by opening the asymmetrically heated pore. A ladder of dsDNA (20–200 bp, 20 bp steps) was injected into the trap. Subsequent flushing of the capillary with pure buffer at a single velocity ( $v_s = 6 \mu\text{m s}^{-1}$ ) revealed the filter's thresholding characteristics—lengths  $\leq 80$  bp flow through the pore whereas longer strands are trapped. **b**, An asymmetric flow pattern is generated by the superposition of the upwards flow and the convection. Thermophoresis pushes the long strands into the downwards flow and traps them. Short strands are subjected to the overall upwards flow and leave the pore. The trapping is a function of the feeding flow speed. **c**, The velocity of the external flow  $v_s$  tunes the fractionation of nucleic acids. As in the experiment before, a DNA ladder was initially introduced at a low flow velocity, which was then sequentially increased. The released DNA was measured using gel electrophoresis. **d**, The fraction of trapped DNA obtained from the electrophoresis gel constitutes a selection landscape of this thermal habitat in favour of long oligonucleotides. The velocity-dependent trapped fraction is described by a fluid dynamics model (see Methods). Error bars reflect the signal-to-noise ratio of the gel images (see Supplementary Fig. 11 for details).

**Differential survival of replicating strands.** Combining all of the above, we show how the joint thermally induced trapping and replication enables this arrangement to overcome Spiegelman's evolutionary dilemma of the degeneration of strand length and therefore loss of genomic information<sup>11</sup>. We followed the composition of a heterogeneous DNA population that replicates continuously inside the open pore. A 2.5 mm short capillary was seeded with a population of unlabelled template DNA strands with identical primer binding sites and a binary length distribution of 36 bp and 75 bp at a concentration of 1 nM each.

A temperature gradient from 61 °C to 94 °C was applied to a continuous upwards flux of template-free PCR buffer that contained nucleotides, polymerase and 7 nM fluorescently labelled primers and was run through the system at a speed of  $6 \mu\text{m s}^{-1}$ . Over the course of the experiment (seven hours), the trapping volume was exchanged approximately 150 times with the template-free feeding

buffer. Aliquots that contained the product of the continuously running reaction were taken from the outflow and analysed using gel electrophoresis. As the primers carried the labels, only replicated DNA strands were detected (Fig. 4c).

We observed that only the long strands were able to replicate sufficiently to withstand the diluting flow through the pore. This determined the increase of the relative concentration of the long, viable strands with respect to the total amount of DNA (Fig. 4d, yellow). The twofold shorter strands became diluted and then extinct.

This competitive replication and selection of two genetic polymers in favour of larger molecular lengths can be understood easily with a simple model. The determinants of the growth kinetics  $dc_i/dt = (rep_i - dil_i)c_i$  for either the short or the long species  $i = \{S, L\}$  are given by the replication rates  $rep_i$  and the dilution rates  $dil_i$ . Expressing the relative concentration of the long strands yields  $c_L/(c_S + c_L) = (1 + Ae^{-\Delta kt})^{-1}$ .  $A = c_S^0/c_L^0$  is the initial

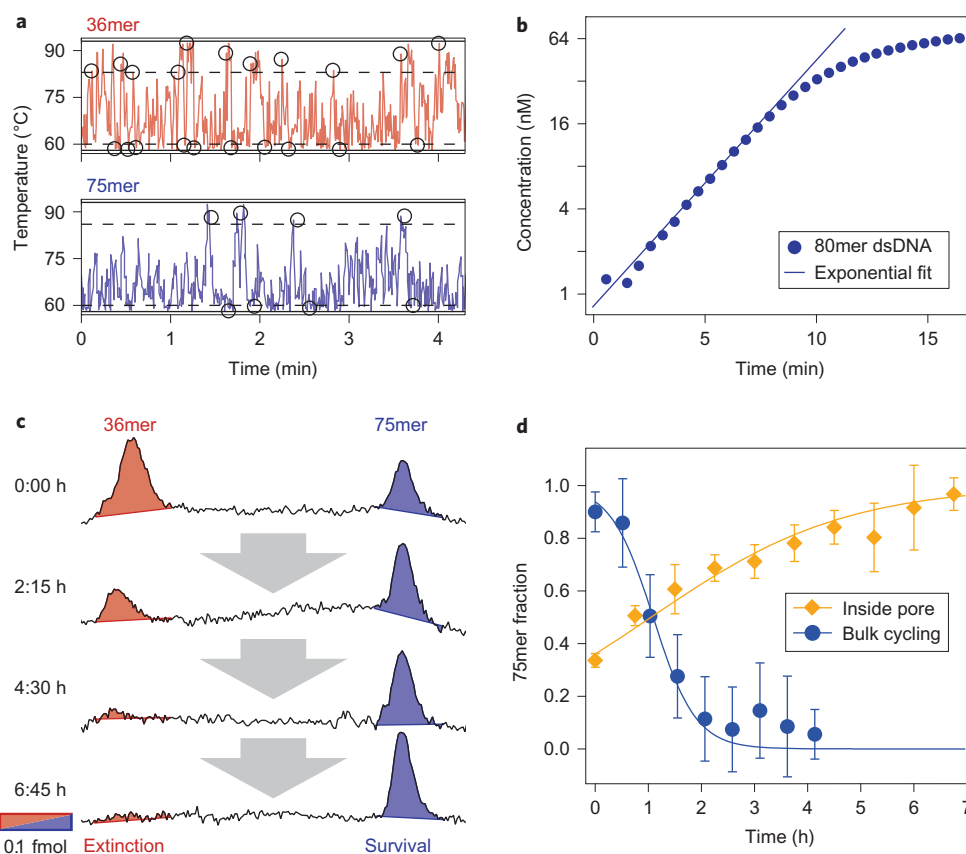


**Figure 4 | Selection of a replicating DNA population that occupies the thermal habitat.** **a**, Strands are subjected to temperature oscillations by the combination of thermophoresis, convection, feeding flow and diffusion. Simulations of stochastic molecule traces show that strands of 75 bp cycle inside the system for 18 minutes on average. In comparison, 36mers, owing to their enhanced diffusion, show faster temperature cycles, but are flushed out of the system after five minutes. **b**, Taq DNA polymerase-assisted replication of 80mer dsDNA by convective temperature cycling. Quantitative SYBR Green I fluorescence measurements show an exponential replication with a doubling time of 102 seconds (see Supplementary Movie 4). **c**, An open pore (see Fig. 1c) was seeded with a binary population of nucleic acids. Quantitative gel electrophoresis revealed sustainable replication for only the long strand. Short strands became diluted and then extinct despite their faster replication. **d**, Relative concentrations of the two competing species inside the thermal habitat. The selection pressure of the thermal gradient altered the composition of the binary population with time (yellow diamonds) in good agreement with an analytical replication model. The absolute fitness values were 1.03 and 0.87 for long and short strands, respectively. Without the thermal gradient, the short oligonucleotides won over the long strands (blue circles), analogous to the Spiegelman experiment. Error bars reflect the signal-to-noise ratio of the gel images (see Supplementary Fig. 11 for details).

concentration ratio and  $\Delta k = (\text{rep}_L - \text{rep}_S) - (\text{dil}_L - \text{dil}_S)$  is the differential growth rate. We experimentally found that, inside the pore, long strands (L) outcompete shorter ones (S) with  $\Delta k = 0.55 \text{ h}^{-1}$  (yellow curve). The length-selective fractionation model (Fig. 3c) confirmed that the shorter strands suffer from a fourfold higher dilution rate as compared to the trapped long strands. This selection of the longer replicating strand works best if the mechanism of replication is inefficient, such that the dilution of the short strand occurs before it can be replicated efficiently.

On the other hand, in a well-mixed situation, and hence in the absence of the selection pressure of the pore, we recovered Spiegelman's dilemma of the tyranny of the short. In a serial dilution experiment using a conventional thermal cycler with dilution rates that reproduce the pore conditions, the long strands died out rapidly with a differential growth rate of  $\Delta k = -2.5 \text{ h}^{-1}$  (Fig. 4d, blue curve).

## Discussion

Our experimental findings conclusively show that, at the expense of dissipating free thermal energy, a habitat is created that drives and sustains the replication of long oligonucleotides by exploiting both convective temperature cycling and a selection pressure

that supports the long over the short sequences. Therefore, heat dissipation enables the pore to overcome Spiegelman's classic problem for *in vitro* replication systems that create ever shorter genetic polymers, which results in the loss of genetic information.

On the hot early Earth, the pore system we describe was probably widespread because of porous, partially metallic volcanic rock, both near the surface and at submarine sites. As metals have a more than 100-fold larger thermal conductivity than water<sup>23</sup>, metallic inhomogeneities near the pores can focus the thermal gradient from centimetres down to a micrometre-sized cleft (Supplementary Fig. 1). The kinetics of replication and selection were realized in the most simple geometrical setting of a single pore section with dimensions of 0.07 mm × 3.5 mm. Metallic inclusions do allow thermal gradients to be focused up to 100-fold to reach the thermal gradients of realistic geological settings (Supplementary Fig. 1). It is, however, important that the steepness of the thermal gradient can be further relaxed by at least one order of magnitude by separating replication and selection into two adjacent pores (Supplementary Fig. 2). At the bottom, a wide pore could provide the necessary temperature difference for replication<sup>24</sup>. At its top, the outflow would be constricted through one or more thin, but longer, selecting

pores. Their increased length of several centimetres instead of 3.5 mm compensates linearly for the reduced temperature difference<sup>13</sup>.

Although the demonstrated length-selective trapping requires a temperature difference to work, the average temperature of the trap is not a critical parameter and can be tuned easily to fit the replication reaction. Therefore, the core mechanism of temperature cycling and selection studied here will also work for replication systems that require colder temperatures, including, for example, ribozymes or Q-beta replicase. However, many early replication systems are likely to rely on high temperatures for temperature-induced strand separation. For the PCR reaction used in the experiment, the strand lengths were highly controlled by the primers. In comparison, reactions that involve ligations have a tendency to extend the strands with partial templating<sup>25</sup> and initiate the length extension of the genetic polymers.

To extend this work to achieve Darwinian evolution in the demonstrated system, the replication process requires a significant mutation rate, including changes of the sequence length. The use of error-prone PCR with deep sequencing is therefore an interesting prospect for future experiments. At this point, the amount inside the pore is less than 1 pg, which prevents such an approach: the necessary strong preamplification would highly bias the obtained sequences and obscure their analysis.

Importantly, the thermophoretic selection pressure applies to each individual molecule of the population. As it is ultimately sensitive to the thermophoretic strength, the selection does not only favour the survival of long strands over short strands—it is possible that this mechanism could be tuned to select for the formation of macromolecular complexes or even for binding of aptamers<sup>26</sup>.

## Conclusion

Our experiments reveal how temperature gradients, the most simple out-of-equilibrium setting, can give rise to local environments that stabilize molecular replication against the entropic tendencies of dilution, degradation and negative length selection. A thermal gradient drives replication of oligonucleotides with an inherent directional selection of long over short sequence lengths. Interestingly, when replication and trapping inside the pore reach their steady state, the newly replicated molecules leave the trap with the feeding flow. This ensures an efficient transfer of the genetic polymers to neighbouring pore systems. Heat dissipation across porous rock was probably in close proximity to other non-equilibrium settings of pH, ultraviolet radiation and electrical potential gradients, all of which are able to drive upstream synthesis reactions that produce molecular building blocks. An exciting prospect of the presented experiments is the possible addition of mutation processes to achieve a sustained Darwinian evolution of the molecular population inside the thermal gradients of the early Earth. Accordingly, the onset of molecular evolution could have been facilitated by the natural thermal selection of rare, long nucleic acids in this geologically ubiquitous non-equilibrium environment.

## Methods

**Temperature gradients.** Temperature gradients were generated across rectangular borosilicate glass capillaries (VitroTubes, VitroCom) with a cross-sectional aspect ratio of 1:20 and a thermal conductivity of  $1.2 \text{ W m}^{-1} \text{ K}^{-1}$ . To this end, two different approaches were followed. (1) For the direct observation of the accumulation effect, glass capillaries were coated with a transparent conducting oxide layer that allowed for one-sided heating at a constant electric power with cooling from the other side. (2) Fractionation and replication experiments were performed in capillaries sandwiched between and thermally connected to temperature-controlled metal surfaces (compare the Supplementary Information and the figures therein for details of both approaches).

**Accumulation-only experiments.** dsDNA was diluted in  $1 \times$  Taq reaction buffer (New England Biolabs) that contained 10 mM Tris-HCl, 50 mM KCl, 1.5 mM  $\text{MgCl}_2$  and 0.1% Tween20, with a pH of 8.3 at room temperature. A dsDNA ladder (10  $\mu\text{g ml}^{-1}$ , 100–1000 bp, ten equidistant bands, weight equalized) was used in combination with  $0.5 \times$  SYBR Green I<sup>27</sup>. The applied temperature gradient from 22 °C

to 88 °C resulted in temperatures from 38 °C to 71 °C inside the capillary (inner dimensions, 100  $\mu\text{m} \times 2,000 \mu\text{m}$  and 70  $\mu\text{m} \times 1,400 \mu\text{m}$ , as specified).

**Fractionation experiments.** A DNA ladder (20–200 bp, ten equidistant bands) was suspended in a  $1 \times$  PCR buffer that included 0.1% Tween20. Fractionation was carried out in a vertically oriented capillary (inner dimensions, 70  $\mu\text{m} \times 1400 \mu\text{m}$ ) with an internal temperature gradient from 39 °C to 73 °C present over a capillary length of 3.5 mm (see the Supplementary Information for the details). The threshold trapping characterization was determined using a constant flow speed. Gradual fractionation was achieved by increasing the flow rate with time using a feedback-controlled syringe pump (neMESYS, Cetoni; see the Supplementary Information for a detailed protocol).

**In vitro selection and replication.** Extracellular selection of replicating DNA strands was studied in a temperature gradient from 61 °C to 94 °C inside a thoroughly cleaned (DNA Away, Molecular BioProducts) capillary (inner dimensions, 70  $\mu\text{m} \times 1,400 \mu\text{m}$ , heated along 2.5 mm) at a mean solvent velocity of  $6 \mu\text{m s}^{-1}$ . DNA replication was facilitated in a commercially available, glycerol-free master mix (fast cycling PCR Kit, Qiagen) that contained Taq polymerase, free nucleotides and standard concentrations of mono- and bivalent salts. The overall efficiency of DNA replication was reduced to less than 8% by means of a low concentration (7 nM) of each 14mer primer (forward (Cy5) and reverse primers; see Supplementary Fig. 7 for the sequences) in the feeding buffer. Unlabelled DNA templates (36mer, 75mer) were seeded into the region of replication through the system's output, leaving the feeding buffer template free. Reaction products that contained the incorporated Cy5 primer from the feeding buffer were extracted from the output of the artificial pore in 1.5  $\mu\text{l}$  aliquots. Controls were performed in a conventional real-time PCR cycler (CFX96, Bio-Rad). A serial dilution experiment was performed to derive the replication efficiencies of the 36mer and 75mer DNA. Temperature cycles emulated the mean temperature cycle of 75mer DNA inside the pore, consisting of three seconds at 94 °C and 14 seconds at 60 °C (Supplementary Fig. 9). Including transition times, the total cycle time was 46.5 s. The initial concentrations were 2 pM (36mer) and 18 pM (75mer) for the PCR templates and 7 nM for the common primers. Every 40 cycles, the sample was diluted by a factor of 20 to yield a dilution rate of  $\text{dil}_s = \text{dil}_l = 5.8 \text{ h}^{-1}$  that counterbalanced the concentration increase of the 36mer DNA within 40 cycles. This scheme prevented a depletion of the primer concentration and ensured that the efficiencies of the PCR reaction stayed constant over all 320 cycles. Replication rates were determined by comparison of the amount of DNA before each dilution using gel electrophoresis (Supplementary Fig. 12). The mean replication rates were determined to be  $\text{rep}_s = (5.8 \pm 0.6) \text{ h}^{-1}$  (36mer) and  $\text{rep}_l = (3.3 \pm 0.4) \text{ h}^{-1}$  (75mer).

Received 28 August 2014; accepted 2 December 2014;  
published online 26 January 2015

## References

- Powner, M. W., Gerland, B. & Sutherland, J. D. Synthesis of activated pyrimidine ribonucleotides in prebiotically plausible conditions. *Nature* **459**, 239–242 (2009).
- Sievers, D. & Von Kiedrowski, G. Self-replication of complementary nucleotide-based oligomers. *Nature* **369**, 221–224 (1994).
- Mansy, S. S. *et al.* Template-directed synthesis of a genetic polymer in a model protocell. *Nature* **454**, 122–125 (2008).
- Wochner, A., Attwater, J., Coulson, A. & Holliger, P. Ribozyme-catalyzed transcription of an active ribozyme. *Science* **332**, 209–212 (2011).
- Paul, N. & Joyce, G. F. A self-replicating ligase ribozyme. *Proc. Natl Acad. Sci. USA* **99**, 12733–12740 (2002).
- Yang, Z., Chen, F., Alvarado, J. B. & Benner, S. A. Amplification, mutation, and sequencing of a six-letter synthetic genetic system. *J. Am. Chem. Soc.* **133**, 15105–15112 (2011).
- Szostak, J. W. The eightfold path to non-enzymatic RNA replication. *J. Syst. Chem.* **3**, 1–14 (2012).
- Pascal, R., Pross, A. & Sutherland, J. D. Towards an evolutionary theory of the origin of life based on kinetics and thermodynamics. *Open Biol.* **3**, 130156 (2013).
- Powner, M. W., Sutherland, J. D. & Szostak, J. W. Chemoselective multicomponent one-pot assembly of purine precursors in water. *J. Am. Chem. Soc.* **132**, 16677–16688 (2010).
- Schrödinger, E. *What is Life?* (Cambridge Univ. Press, 1944).
- Mills, D. R., Peterson, R. L. & Spiegelman, S. An extracellular Darwinian experiment with a self-duplicating nucleic acid molecule. *Proc. Natl Acad. Sci. USA* **58**, 217–224 (1967).
- Lay, T., Hernlund, J. & Buffett, B. A. Core–mantle boundary heat flow. *Nature Geosci.* **1**, 25–32 (2008).
- Baaske, P. *et al.* Extreme accumulation of nucleotides in simulated hydrothermal pore systems. *Proc. Natl Acad. Sci. USA* **104**, 9346–9351 (2007).
- Budin, I., Bruckner, R. J. & Szostak, J. W. Formation of protocell-like vesicles in a thermal diffusion column. *J. Am. Chem. Soc.* **131**, 9628–9629 (2009).
- Mast, C. B., Schink, S., Gerland, U. & Braun, D. Escalation of polymerization in a thermal gradient. *Proc. Natl Acad. Sci. USA* **110**, 8030–8035 (2013).

16. Clusius, K. & Dickel, G. Trennung von Flüssigkeitsgemischen mittels kombinierter Thermodiffusion und Thermosiphonwirkung. *Naturwissenschaften* **26**, 546 (1938).
17. Debye, P. Zur Theorie des Clusius'schen Trennungsverfahrens. *Annal. Phys.* **428**, 284–294 (1939).
18. Piazza, R. & Guarino, A. Soret effect in interacting micellar solutions. *Phys. Rev. Lett.* **88**, 208302 (2002).
19. Duhr, S. & Braun, D. Why molecules move along a temperature gradient. *Proc. Natl Acad. Sci. USA* **103**, 19678–19682 (2006).
20. Krishnan, M., Ugaz, V. M. & Burns, M. A. PCR in a Rayleigh–Benard convection cell. *Science* **298**, 793 (2002).
21. Mast, C. B. & Braun, D. Thermal trap for DNA replication. *Phys. Rev. Lett.* **104**, 188102 (2010).
22. Rajamani, S. *et al.* Effect of stalling after mismatches on the error catastrophe in nonenzymatic nucleic acid replication. *J. Am. Chem. Soc.* **132**, 5880–5885 (2010).
23. Tritt, T. M. *Thermal Conductivity: Theory, Properties and Applications* (Kluwer Academic/Plenum, 2004).
24. Braun, D., Goddard, N. L. & Libchaber, A. Exponential DNA replication by laminar convection. *Phys. Rev. Lett.* **91**, 158103 (2003).
25. Fernando, C., Von Kiedrowski, G. & Szathmáry, E. A stochastic model of nonenzymatic nucleic acid replication: “Elongators” sequester replicators. *J. Mol. Evol.* **64**, 572–585 (2007).
26. Baaske, P., Wienken, C. J., Reineck, P., Duhr, S. & Braun, D. Optical thermophoresis for quantifying the buffer dependence of aptamer binding. *Angew. Chem. Int. Ed.* **49**, 2238–2241 (2010).
27. Wilhelm, J. & Pingoud, A. Real-time polymerase chain reaction. *ChemBioChem* **4**, 1120–1128 (2003).
28. Kelley, D. S. *et al.* An off-axis hydrothermal vent field near the Mid-Atlantic Ridge at 30° N. *Nature* **412**, 145–149 (2001).

### Acknowledgements

We thank N. Osterman and C. Mast for the preliminary trapping experiments and discussions, M. Herzog and M. Reichl for thermophoresis measurements and S. Krampf for help with the gel electrophoresis. Financial support from the NanoSystems Initiative Munich, the Simons Collaboration on the Origin of Life, the Ludwig-Maximilians-Universität Munich Initiative Functional Nanosystems, the SFB 1032 Project A4 and the European Research Council (ERC) Starting Grant is acknowledged.

### Author contributions

M.K., L.K. and S.L. contributed equally to this work and performed the experiments. M.K., L.K., S.L. and D.B. conceived and designed the experiments, analysed the data and wrote the paper.

### Additional information

Supplementary information is available in the [online version](#) of the paper. Reprints and permissions information is available online at [www.nature.com/reprints](http://www.nature.com/reprints). Correspondence and requests for materials should be addressed to D.B.

### Competing financial interests

The authors declare no competing financial interests.

# HEAT FLUX ACROSS AN OPEN PORE ENABLES THE CONTINUOUS REPLICATION AND SELECTION OF OLIGONUCLEOTIDES TOWARDS INCREASING LENGTH

Moritz Kreysing<sup>1,2,\*</sup>, Lorenz Keil<sup>1,\*</sup>, Simon Lanzmich<sup>1,\*</sup> and Dieter Braun<sup>1</sup>

<sup>1</sup> Systems Biophysics, Physics Department, Center for Nanoscience,  
Ludwig-Maximilians-Universität München, 80799 Munich, Germany

<sup>2</sup> now: Max Planck Institute of Molecular Cell Biology and Genetics, Dresden, Germany

\*: contributed equally

## Table of Contents

<b>Supplementary Methods</b>	<b>3</b>
Temperature gradients i) Ohmic heating with a transparent electrode.....	3
Temperature gradients ii) Ohmic heating at monitored temperatures.....	3
Microfluidics.....	4
Imaging of fluorescently labelled oligonucleotides.....	4
Gel electrophoresis and documentation.....	4
Fractionation experiments.....	5
Quantitative gel analysis.....	5
Replication model.....	6
Diffusion and screening length parameters of DNA.....	7
Computer simulations and analytical trapping model.....	7
Calculation of temperature cycling times.....	8
Modelling of fractionation experiments.....	8

<b>Supplementary Figures</b>	<b>9</b>
Supplementary Fig. S1   Focussing of a temperature gradient in a millimetre-sized pore.....	9
Supplementary Fig. S2   Separation of accumulation and thermal cycling in multipore system..	10
Supplementary Fig. S3   Experimental set-up to generate temperature gradients across rectangular borosilicate capillaries by electrically heating a transparent electrode.....	11
Supplementary Fig. S4   Cross-sectional drawings of flow-through set-up employed for fractionation and selection & replication experiments (Figures 3, 4), side and top view.....	12
Supplementary Fig. S5   Injection of a DNA pulse for the fractionation experiments shown in Figure 3.....	13
Supplementary Fig. S6   Determination of critical trapping velocities for each 20 bp ladder fragment.....	14
Supplementary Fig. S7   Analytic fit functions for the Soret and diffusion coefficients of DNA and RNA based on published measurements of short DNA.....	15
Supplementary Fig. S8   Visualisation of random walk simulations of 36 mer (left group) and 75 mer (right group) DNA inside a 70 $\mu\text{m}$ wide, asymmetrically heated pore.....	16
Supplementary Fig. S9   Thermal cycle times of individual nucleotide particles inferred from trajectories.....	17
Supplementary Fig. S10   Temperature cycle statistics obtained from random walk simulations.	18
Supplementary Fig. S11   Quantification of native polyacrylamide gel data from the selection and replication experiment presented in Fig. 4 b, d.....	19
Supplementary Fig. S12   Quantification of native polyacrylamide gel data from the serial dilution experiment presented in Fig. 4d.....	20
<b>Supplementary Videos</b>	<b>21</b>
<b>Supplementary References</b>	<b>23</b>

## Supplementary Methods

### Temperature gradients i) Ohmic heating with a transparent electrode

Glass capillaries were plasma cleaned and coated with a thin layer of indium tin oxide (ITO, Supplementary Fig. S3) in a radio frequency sputtering chamber (LS320, Von Ardenne, Germany)<sup>1-3</sup>, equipped with a custom-built translation stage. Sputtering under an argon atmosphere for 40 minutes at 30 W and subsequent heat treatment for 30 minutes at 250 °C resulted in a typical sheet resistance of 12 Ohms per square and high optical quality. The one-side coated capillaries were glued onto a commercially available water CPU cooler (Innovatek, Germany) using a thin film of silver-filled thermally conducting epoxy (Arctic Silver, Arctic Silver, USA). The ITO-coated side of the capillary was electrically connected to a digitally controlled power supply (6010A, Agilent, USA) via copper wires and conductive paint (Busch5900, Busch, Germany). Temperature gradients across the capillary were established through electric heating at constant power, with the cooled side of the capillary being controlled by a water bath (F31-C, Julabo, USA) operating at constant temperature. The thermal response of the capillary was calibrated with a thermochromic dye (70C black, Sintal Chemie, Germany) that was put on top of the capillary.

### Temperature gradients ii) Ohmic heating at monitored temperatures

Glass capillaries were sandwiched between plan sapphire windows (thickness: 100  $\mu\text{m}$ , Sappro, Germany) on copper substrates using a thermally coupling adhesive (TC-2707, 3M, USA, cf. Supplementary Fig. S4). This ensured accurate temperature conditions in experiments requiring intra-capillary temperatures as high as 90 °C to 100 °C. Heating was achieved by an Ohmic resistor connected to a computer controlled power supply. A Peltier element on a water-based CPU cooler was used for cooling. During the experiments, temperatures were measured on both copper surfaces by thermocouples in a LabVIEW-based computer environment, and stabilised by a PID-controlled feedback loop acting on the cooling side ( $\pm 50$  mK)<sup>4</sup>, resulting in stable temperature conditions also on the heated side ( $\pm 1$  K long term drift). Heating was applied along a 2.5–3.5 mm long section of the capillary.

### Microfluidics

Glass capillaries were connected to a feedback controlled syringe pump (neMESYS, Cetoni, Germany), via high purity PFA tubing (HPFA+, Upchurch Scientific, USA), and tightly matched silicon seals. Microfluidic distances between the heated region of the capillary and its accessible output measured 3  $\mu\text{l}$  to 5  $\mu\text{l}$ , and were determined with a precision higher than 0.2  $\mu\text{l}$  prior to fractionation experiments and the seeding of the pore in the selection and replication experiment. Degassing of this microfluidic system was done by flushing isopropyl alcohol followed by degassed PCR reaction buffer (Standard Taq Reaction Buffer, New England Biolabs, Germany) using an overpressure of several bars. Crucially, all assays also had to be degassed carefully prior to loading into the system in order to avoid air bubble formation during the experiments. This was achieved by heating 200  $\mu\text{l}$  sample tubes to 88 °C. After one minute, a mechanical shock was applied to induce to the formation of gas bubbles. Consequently, the temperature was kept at 88 °C for five minutes, followed by an increase to 94 °C for four minutes. Finally, gas bubbles were released from the tube walls by vortexing for three seconds. In order to avoid re-saturation of the samples with oxygen from the air, tubes were maintained at 90 °C during injection of the assay into the system.

### Imaging of fluorescently labelled oligonucleotides

Fluorescent imaging of DNA was realised with a 90°-tilted upright microscope (Axioscope A1, Zeiss), using a 2.5 $\times$  objective (Plan-Neofluar 2.5 $\times$  0.075 NA, Zeiss, Germany), equipped with a CCD camera (1400, PCO, Germany) and two alternating light-emitting diodes (LED 470 nm, LED 625 nm, Thorlabs, USA) in combination with a dual band filter set (Dual band FITC / Cy5, AHF, Germany).

### Gel electrophoresis and documentation

Native gel electrophoresis was performed in 12.5 % polyacrylamide gels inside a 1 $\times$  TBE buffer at electric field strengths of 60 V/cm and 30 °C for 13 minutes. After running, the gels were stained by incubation in fresh 1 $\times$  solutions of SYBR Green I (Invitrogen, Germany) in TBE buffer for four minutes followed by a one minute washing step in pure TBE. Imaging of SYBR Green I stained gels was done by CCD photography through a green bandpass filter (520 nm, 10 nm FWHM, Newport, Germany) under spectrally filtered (470 nm, 10 nm FWHM, Thorlabs, USA) light emitting diode excitation (LED 470 nm, Thorlabs, Germany).

Denaturing gel electrophoresis was performed after a standard protocol<sup>5</sup>. In short, DNA samples were denatured in a formamide glycerol buffer at 95 °C for 2 minutes, followed by shock cooling on ice. Then, the samples were loaded into 12.5 % polyacrylamide gels containing 50 % urea. After a 5 minutes pre-run at 7.5 V/cm, the samples were separated by an electric field of 60 V/cm in 45 °C–50 °C warm TBE buffer for 13 minutes.

For analysis, the gels containing the Cy5 labelled reaction products from the extra-cellular selection and replication experiment were illuminated with two spectrally filtered light emitting diodes (LED 625 nm, filter 630 nm, 10 nm FWHM, Thorlabs, Germany). Detection was done through a pair of high quality interference filters (bandpass 692±20 nm, OD6 blocking, Edmund Optics, USA, and bandpass 700±35 nm, OD 2 blocking, Newport, USA, resulting in an excitation rejection of OD8+) by an actively cooled CCD camera (Orca 03-G, Hamamatsu, Japan).

### Fractionation experiments

A weight equalised double stranded DNA ladder (10 equidistant bands, 20 bp–200 bp, Carl Roth, Germany) was separated from its loading dye by ethanol precipitation and resuspended at a final concentration of 0.25 µg/µl in 1× PCR buffer containing 10 mM Tris-HCl, 50 mM KCl, 1.5 mM MgCl<sub>2</sub>, and 0.1 % Tween20 with a pH of 8.3 at room temperature. After degassing the DNA-free microfluidic system, the DNA ladder was sucked into a reservoir with an inlet just before the region of the temperature gradient (cf. Supplementary Fig. S5). After flushing the main channel with DNA free buffer again, a 1.5 µl pulse of the DNA ladder was injected into the trapping region, followed by the constant flow of pure buffer driving the fractionation. Experiments were carried out in a capillary (internal dimensions: 70 µm×1400 µm) with a heated region of 3.5 mm length and a temperature gradient ranging from 39 °C to 73 °C. A fractionation run with higher terminal velocities than in Figure 3c is shown in Supplementary Fig. S6c.

### Quantitative gel analysis

Gel image quantification (as shown in Supplementary Fig. S11, S12) was done with a custom LabVIEW program, after point-like outliers have been removed using NIH ImageJ<sup>6</sup>. Before integrating the intensities, images were corrected for inhomogeneous illumination. To improve the signal to noise ratio, the intensity of each gel lane was then integrated along the horizontal axis. Further, a local linear background was subtracted from each gel band (shaded regions in

Supplementary Fig. S11d, S12c). The uncertainty of this integral was estimated using the standard deviation of the values around the base points of the linear background.

### Replication model

The amplification of a target DNA sequence using PCR is described by  $c(n) = c_0 \cdot (1+E)^n$ , where  $n$  denotes the number of cycles and  $E$  the PCR efficiency. Under the replication conditions in our experiment, molecules are also subjected to a continuous outflow. The latter is modelled by a dilution rate per unit time  $dil$ . In a continuous time description, the replication rate per unit time is  $rep = \ln(1+E)/t_c$  with the temperature cycle time  $t_c$  of the PCR reaction. This leads to a combined growth equation for each species  $i$  given by  $dc_i/dt = c_i(rep_i - dil_i)$ . Its solution is  $c(t) = c_i^0 \cdot e^{(rep_i - dil_i)t}$ , the relative concentration of 75mer DNA is given by  $c_L/(c_S + c_L) = c_L^0 \cdot e^{k_L t} / (c_L^0 \cdot e^{k_L t} + c_S^0 \cdot e^{k_S t})$ , with  $k_i = (rep_i - dil_i)$ . Defining  $A = c_S^0/c_L^0$  as the ratio of the initial concentrations of short versus long strands, and the differential growth rate  $\Delta k = (rep_S - rep_L) - (dil_S - dil_L)$ , this can be simplified to  $c_L/(c_S + c_L) = (1 + A \cdot e^{\Delta k \cdot t})^{-1}$ .

Taking into account separately determined parameters for temperature gradients, Soret coefficients, diffusion coefficients, and inflow velocities, the fluid-dynamic model yields dilution rates of  $dil_L = 3.2 \text{ h}^{-1}$  and  $dil_S = 12.5 \text{ h}^{-1}$  for the selection and replication experiment. Replication rates were experimentally determined in a PCR cycler set up to match temperature cycling rates inside the pore (compare Supplementary Fig. S9 for their determination). We found replication rates of  $rep_L = (3.3 \pm 0.4) \text{ h}^{-1}$  for the long strands and  $rep_S = (12.05 \pm 0.06) \text{ h}^{-1}$  for the short strands. Interestingly, in the absence of dilution, the short strand replicates 3.7 times faster inside the pore than the longer strand, partly reflecting its a priori evolutionary advantage of a higher replication efficiency  $E$  (as described by Spiegelman, cf. also Supplementary Fig. S12). In addition, the short strand experiences faster temperature cycles (19 s) than the long strand (44 s) due to its higher diffusive mobility.

The absolute fitness for a specific genotype is defined by the ratio of individual (strands) before and after selection. The fitness is a binary distribution (zero or one) when evaluated on time scale that the flow needs to run through the pore. During the lifetime  $\tau = 18.8 \text{ min}$  of long strands in the pore defined by on/off-rate decay  $c/c_0 = 1/e$ , the population of long strand growths around 3%, and the population of short strands shrinks by 13%, leading to absolute fitness values of 1.03 and 0.87 for the long and short strands respectively. If the time axis is scaled by the lifetime of the short strands, these numbers would read 1.01 and 0.96, respectively.

Taken together, the higher replication rate of the short strand is overcompensated by the length selective dilution. Using the here determined rates in our exponential growth model yields relative growths of  $c_L(7h)/c_L(0) \approx 2.0$  and  $c_S(7h)/c_S(0) \approx 0.04$  for short and long strands, respectively. This is in good agreement with the experimental results of the selection and replication experiment of  $c_L(7h)/c_L(0) = 1.7 \pm 0.3$  and  $c_S(7h)/c_S(0) = 0.1 \pm 0.1$ .

### Diffusion and screening length parameters of DNA

The Debye length is a major determining parameter for the strength of thermophoresis. It was estimated as  $\lambda_{DH} = 1.30$  nm for the used PCR buffer (10mM TRIS, 50mM KCl, 1.5mM MgCL<sub>2</sub>) at 75°C. Measurements of DNA at this Debye length were interpolated from the previously measured two-dimensional data set<sup>7</sup>. As seen in Supplementary Fig. S7a, the Soret coefficients of single and double stranded DNA do not significantly differ. Interestingly, RNA shows very similar thermophoretic properties<sup>7</sup>. We therefore used all measured values and interpolate them with a square root function, resulting in  $S_T = -0.0063 + 0.0115 \cdot (\#bases)^{0.5}$ . Here,  $\#bases$  is the number of bases on a single strand. A very similar approach of fitting was used previously<sup>8</sup>.

To infer the diffusion coefficient from the same measurements<sup>9</sup>, the radius of dsDNA was fitted from the same data set as plotted in Supplementary Fig. S7b<sup>7</sup>. The radius shows good agreement with a line fit according to  $R = (0.8 + \#bases \times 0.059)$  nm. Based on the same measurements, the hydrodynamic radius is then translated into the diffusion coefficient by the Einstein relation with the viscosity taken at the temperature of 75°C, resulting in a diffusion coefficient for the COMSOL simulation given by  $D = 6.69 \times 10^{-19} / (8 \times 10^{-10} + (\#bases) \times 5.9 \times 10^{-11})$  m<sup>2</sup>/s.

### Computer simulations and analytical trapping model

Non-stochastic computer simulations of the nucleotide accumulation in a thermal gradient were performed in COMSOL Multiphysics, similar to simulations published before<sup>7</sup>. Additionally, a custom computer program was used to access stochastic information of particle motion which is relevant to calculate cycling rates. Here, individual particles were traced on a biased random walk trajectory inside the combined temperature and velocity fields. As a basis for this stochastic simulation, COMSOL provided the temperature field (conductive heat transfer module) and the velocity field (incompressible Navier-Stokes module).

### Calculation of temperature cycling times

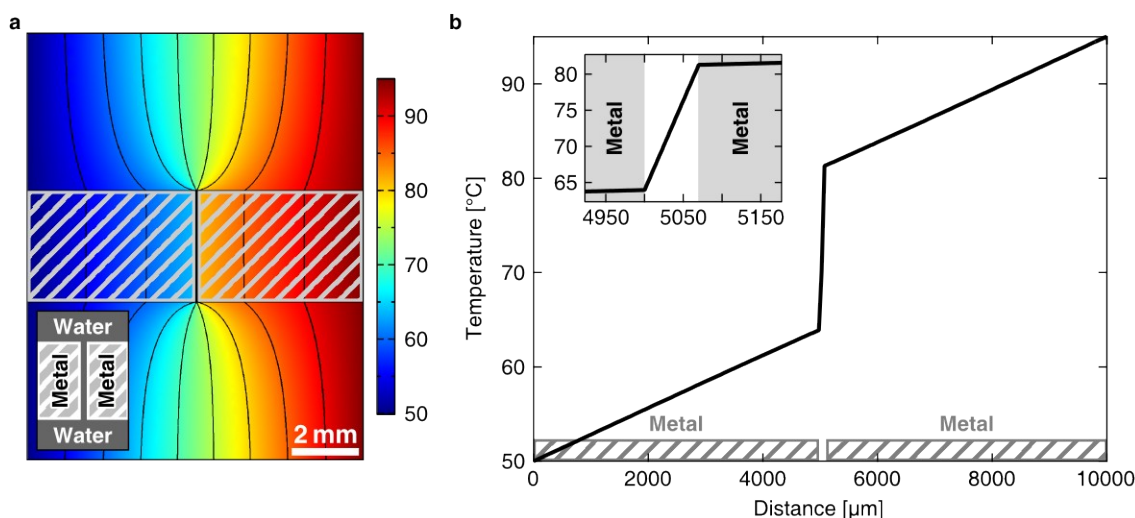
Typical results of these stochastic particle tracing simulations are visualised in Supplementary Fig. S8, showing individual trajectories for 36mer and 75mer DNA in the trapping geometry relevant to the selection and replication experiment of Fig. 4d. Using these trajectories, statistical data on thermal cycles and particle lifetimes can be obtained. For each DNA species, a temperature cycle is defined using two threshold temperatures: an annealing temperature  $T_A$  and a denaturation temperature  $T_D$ . A temperature cycle is defined as the time it requires for a particle to go from  $T_A$  to  $T_D$  and back. Supplementary Fig. S9 shows length resolved DNA strand trajectories and cycling parameter extracted from it.

The thermal cycling in the pore is comparable to that of a standard PCR protocol with short denaturation times and a longer annealing/elongation step. Compared to the 75mer DNA, the 36mer cycles faster between the warm and cold sides of the pore, which is due to its higher diffusion and lower Soret coefficients. Thermal cycling statistics for the two DNA species and different influx velocities is presented in Supplementary Fig. S10. Notably, the cycling time depends only weakly on the influx velocity, whereas the total number of cycles is determined by time the particles residence time inside the pore before being flushed out.

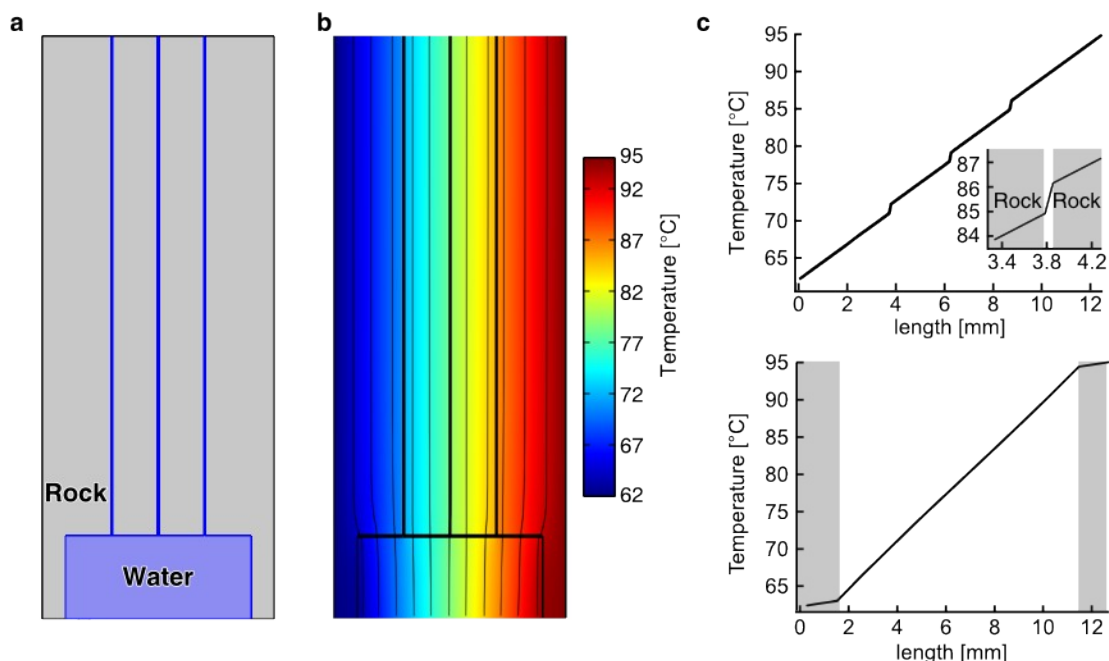
### Modelling of fractionation experiments

Simulations of the fractionation of a DNA ladder, as presented in Fig. 3, required multiple steps. First, we simulated the length-dependent propagation and trapping of a mixed-length DNA pulse through the trap for different influx velocities. From this data, we calculated the length distribution of strands that have been flushed out after a given time. The time steps were chosen to match the increases of inflow velocities presented in Supplementary Fig. S6a,b. For each velocity step, the concentration of the DNA leaving the trap was normalised to the step duration.

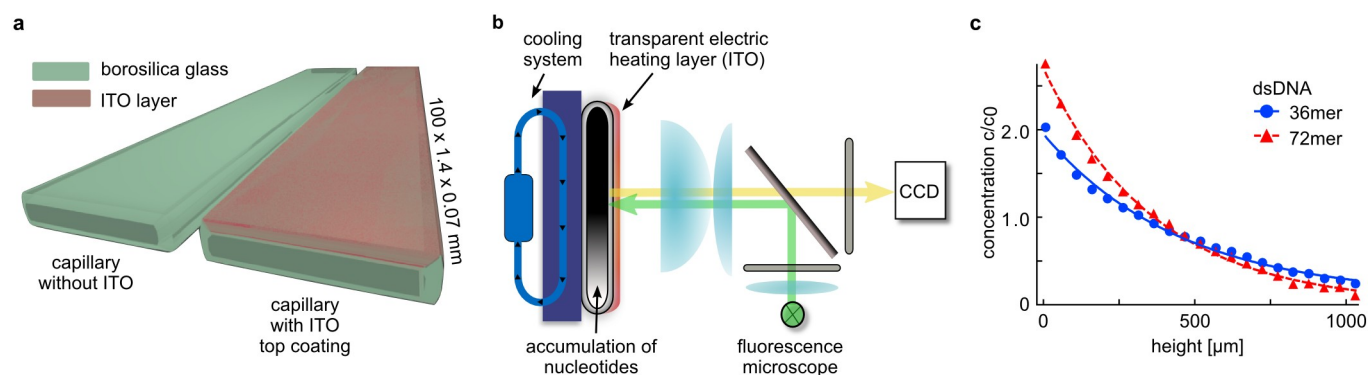
## Supplementary Figures



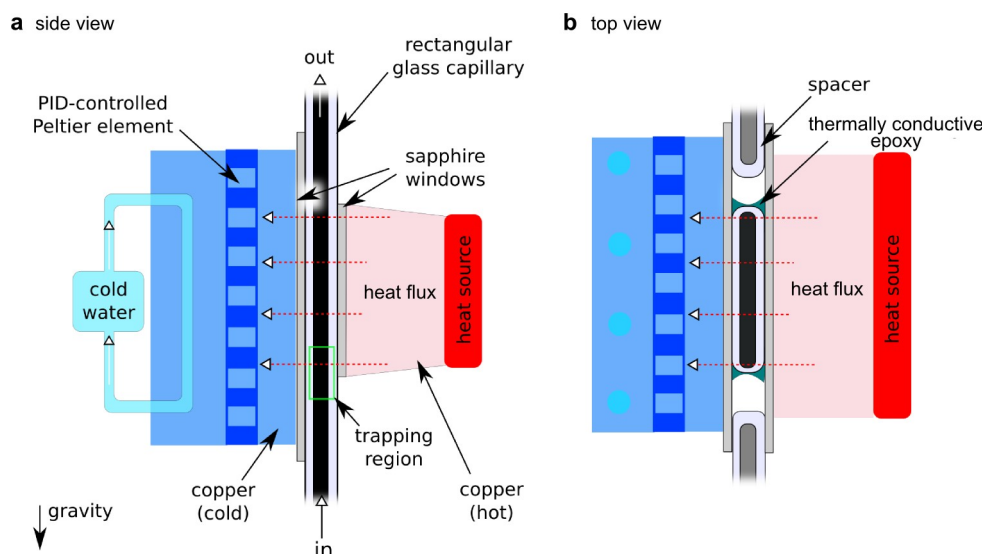
**Supplementary Fig. S1 | Focussing of a temperature gradient in a millimetre-sized pore.** **a**, Millimetre-sized metal inclusions (grey hatched) focus a temperature gradient across a millimetre-sized pore. As metals show about 100-fold higher thermal conductivities than water, the temperature gradient is strongly focussed to the 70 μm gap between the two inclusions. **b**, Horizontal cut along the metal inclusions in panel a. Inside the gap, the temperature gradient is increased to 250 K/mm, compared to 4.5 K/mm in the bulk water. For the calculation, thermal conductivities of 0.58 W/m·K for water and 50 W/m·K for the metal inclusion have been used. The latter is on the lower end of the range for metals, with copper having the highest (400 W/m·K).



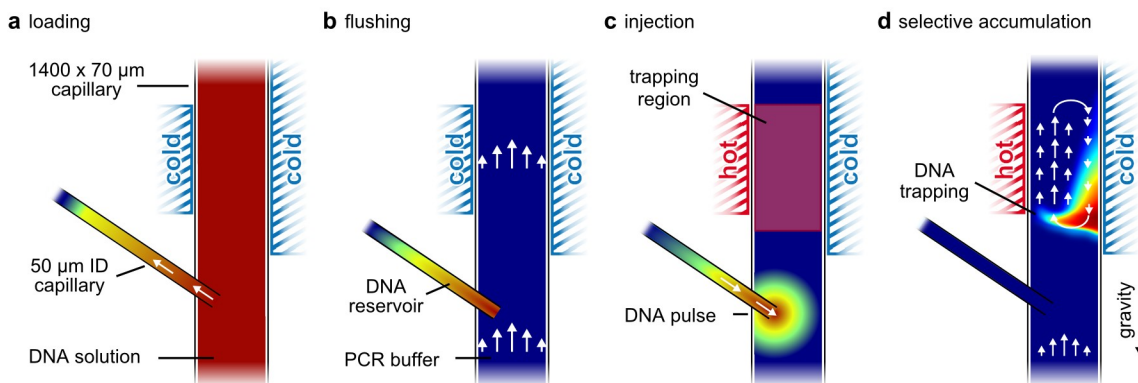
**Supplementary Fig. S2 | Separation of accumulation and thermal cycling in multipore system.** **a**, A multipore system combining a large 1 cm sized pore with multiple 70 μm small sized pores. The small pores with a length of 3 cm are able to accumulate DNA 10<sup>3</sup>-fold and the accumulation grows exponentially with the length of the pore system. The large pore exhibits a strong convection flow which shuttles the molecules between warm and cold with velocities up to 4.8 cm/s. **b**, By assuming a thermal conductivity of 5 W/m K for porous rocks, a temperature gradient of 31 K and 1.2 K is formed along the large and small pore, respectively.



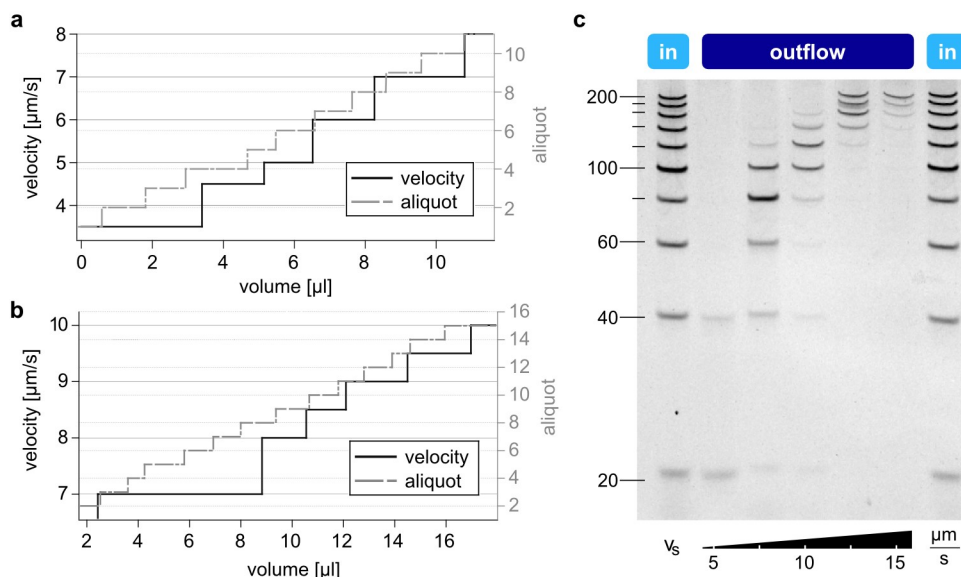
**Supplementary Fig. S3 | Experimental set-up to generate temperature gradients across rectangular borosilicate capillaries by electrically heating a transparent electrode.** **a**, Schematics of the capillary before and after coating with a transparent layer of indium tin oxide (ITO, here red). **b**, Capillary thermally connected to a vertically oriented heat sink (blue). The electrically generated heat from the ITO layer (red) flows through the capillary, giving rise to the accumulation of nucleotides at its bottom. Time-resolved accumulation is recorded by a standard wide-field fluorescent microscope. **c**, Height-resolved concentration profiles of FAM-labelled dsDNA templates 36 mer and 72 mer reveal exponential accumulation characteristics with a stronger spatial confinement of longer oligonucleotides. The experiment was carried out in a capillary with internal dimensions of  $70\ \mu\text{m} \times 1400\ \mu\text{m}$  and a temperature gradient ranging from  $23^\circ\text{C}$  to  $58^\circ\text{C}$  at the outer walls and  $31^\circ\text{C}$  to  $50^\circ\text{C}$  at the inner walls of the capillary.



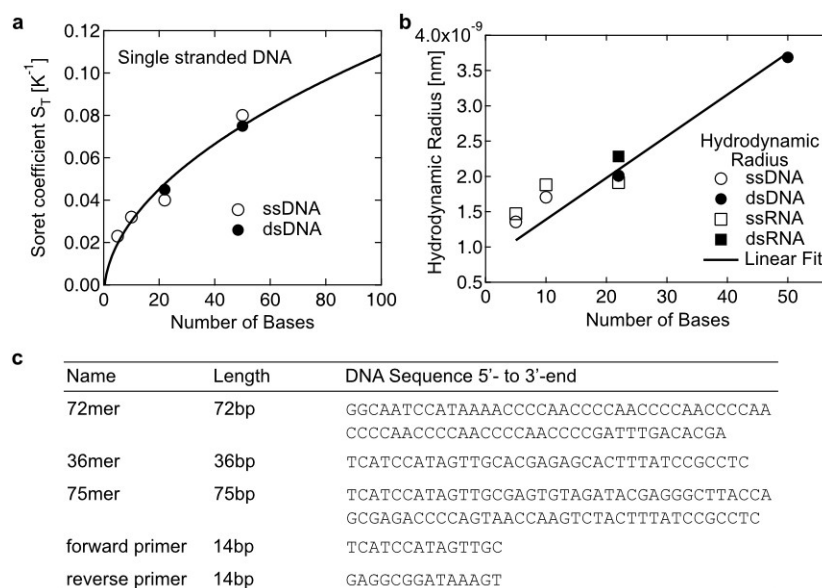
**Supplementary Fig. S4 | Cross-sectional drawings of flow-through set-up employed for fractionation and selection & replication experiments (Figures 3, 4), side and top view.** A rectangular glass capillary is sandwiched between two sapphire windows. Thermal coupling is achieved by thermally conductive epoxy adhesives. The heat created by a constantly powered resistor on the red side flows through the capillary into a PID-regulated heat sink. Spacer capillaries ensure a homogeneous temperature gradient.



**Supplementary Fig. S5 | Injection of a DNA pulse for the fractionation experiments shown in Figure 3.** **a**, Concentrated DNA was pulled from the main channel into a 50  $\mu\text{m}$  capillary, serving as a DNA reservoir. **b**, The DNA solution inside the main capillary is replaced by PCR buffer solution. **c**, Injection of a 1.5  $\mu\text{l}$  pulse of DNA below the trapping region after applying a temperature gradient. **d**, External inflow exerts selection pressure on oligonucleotides.

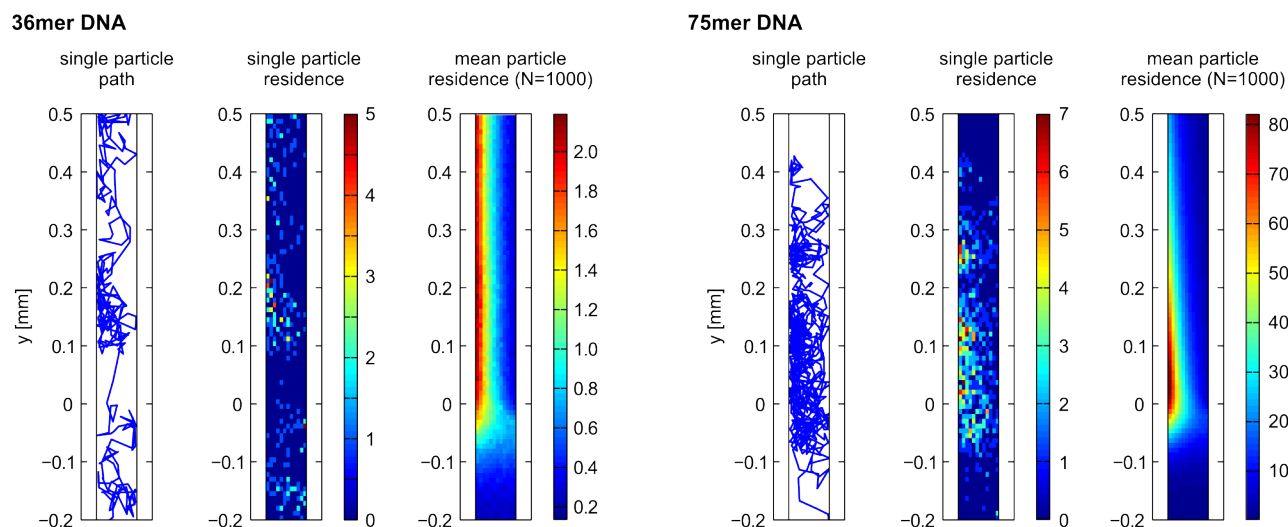


**Supplementary Fig. S6 | Determination of critical trapping velocities for each 20 bp ladder fragment.** Fractionated DNA was obtained from the output of the microfluidic system in volumes between 0.9-1.5  $\mu\text{l}$  and assigned to the step-wise increased velocities. **a**, The influx was gradually increased from 3.5 nl/s to 10 nl/s. At an inflow of 3.5  $\mu\text{m/s}$ , 4.5  $\mu\text{m/s}$ , 5  $\mu\text{m/s}$ , 6  $\mu\text{m/s}$  and 7  $\mu\text{m/s}$ , DNA fragments with a length of 20bp, 40bp, 60bp, 80bp and 100bp started to be flushed out of the trapping region, respectively. **b**, At an inflow of 7  $\mu\text{m/s}$ , 8  $\mu\text{m/s}$ , 8.5  $\mu\text{m/s}$  and 9  $\mu\text{m/s}$ , DNA fragments with a length of 100bp, 120bp, 140bp and 160bp were flushed out, respectively. **c**, Gel electrophoresis of thermally fractionated double stranded DNA ladder (20-200bp) under same conditions as data presented in main text (Fig. 3c), but at coarser velocity steps and with a wider range of inflow velocities  $v_s$ .

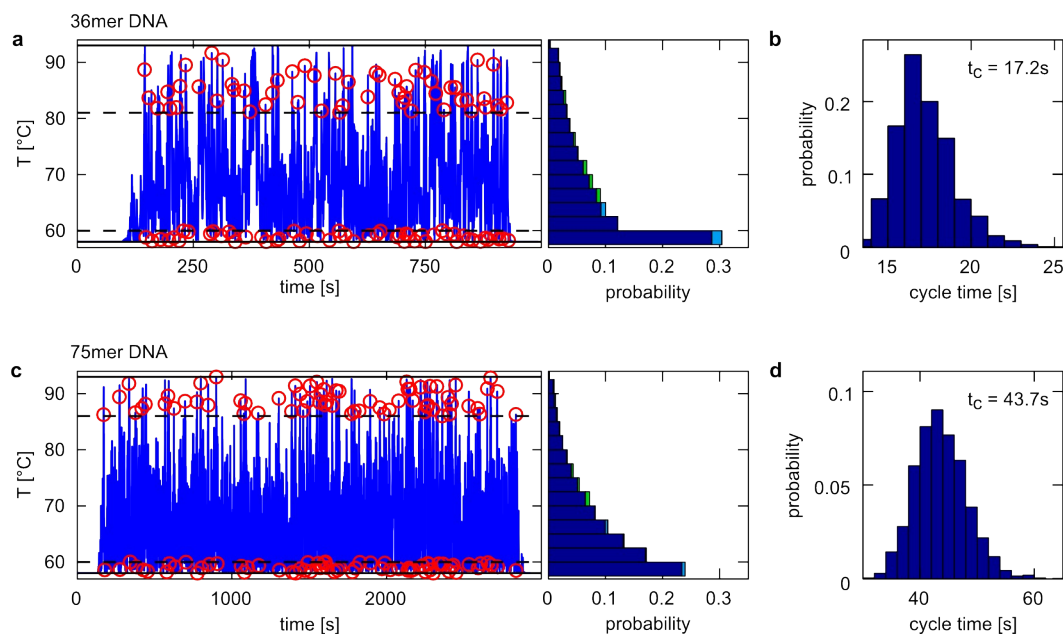


**Supplementary Fig. S7 | Analytic fit functions for the Soret and diffusion coefficients of DNA and RNA based on published measurements of short DNA.**

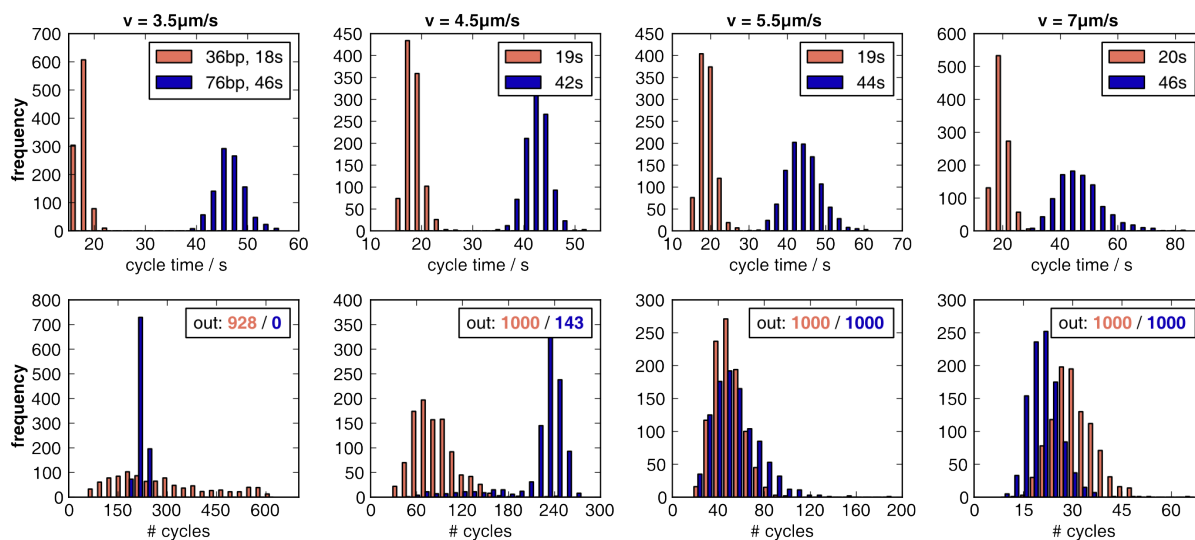
**a**, The fit of the Soret coefficient is used as input parameter for the fluid dynamic computer simulation of the thermal trap. **b**, Hydrodynamic radius of single and double-stranded DNA/RNA. **c**, Sequences of 72mer, 36mer, 75mer, and forward and reverse primers.



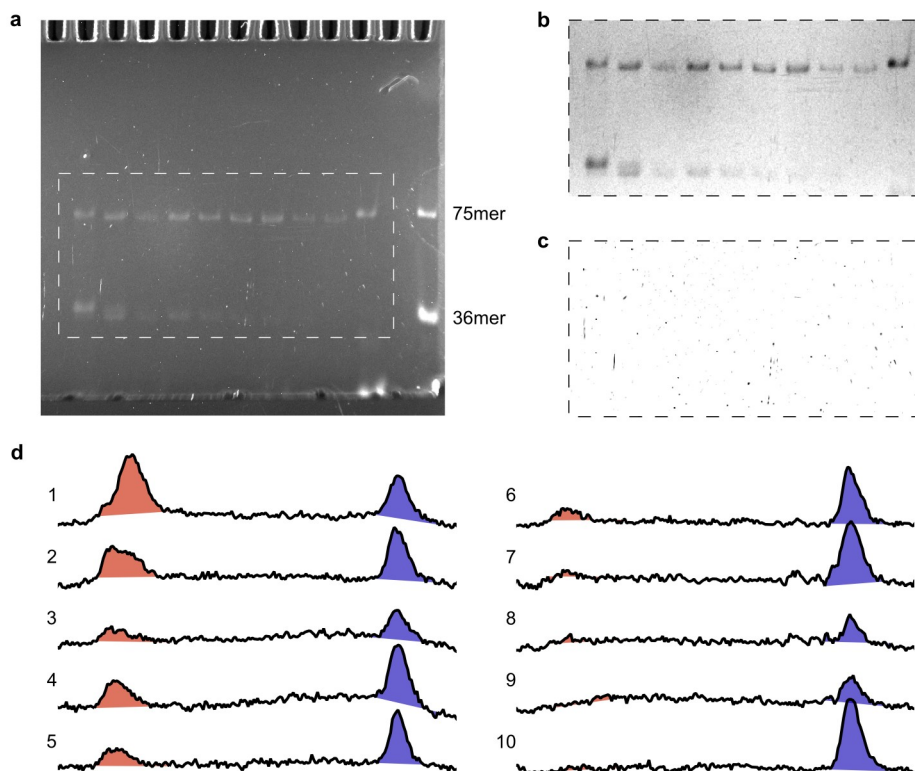
**Supplementary Fig. S8 | Visualisation of random walk simulations of 36 mer (left group) and 75 mer (right group) DNA inside a 70  $\mu\text{m}$  wide, asymmetrically heated pore.** A mean influx velocity of 4  $\mu\text{m/s}$  is applied from below. Individual panels show a single particle trajectory (left), the corresponding single particle density function (middle), and the mean concentration profile from 1000 independent simulations (right). The trajectories cover the first 500 s of the simulations. Note the different colour scales for the short and the long strand. For the depicted influx velocity, the longer DNA species is trapped, while the shorter strand is not.



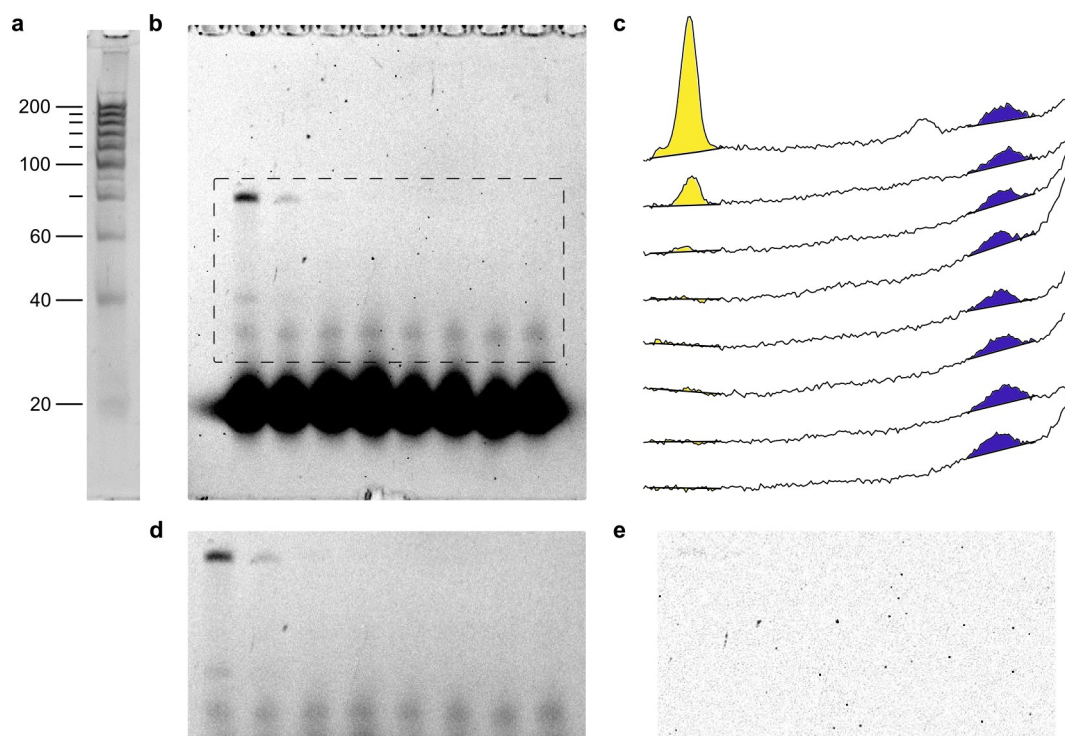
**Supplementary Fig. S9 | Thermal cycle times of individual nucleotide particles inferred from trajectories.** The underlying simulation has been performed for  $N=1000$  particles at an influx velocity of  $5.5\ \mu\text{m/s}$ . **a, c**, Temperature experienced during the lifetime of an individual particle. The dashed lines indicate the temperatures  $T_A$  and  $T_D$ . Red circles mark all entries into the regions colder than  $T_A$  and hotter than  $T_D$ , respectively. The temperature histograms summarise the time-resolved data of the full set of particles. Light blue (green) areas indicate negative (positive) deviations of the histogram for the single particle from that of the full set. **b, d**, Cycle time histograms. The mean cycle time is indicated in the top right corner.



**Supplementary Fig. S10 | Temperature cycle statistics obtained from random walk simulations.**  $N=1000$  particles have been simulated for 10.000 s. **Top row:** Particle cycle time distributions. The cycling times depend only weakly on the inflow rate. In all cases, short strands (red) cycle faster than long strands (blue) due to their higher mobility and lower affinity to the cold side. **Bottom row:** Particle cycle counts. The numbers in the top right of the diagrams indicate the number of particles that left the simulation volume, colour coded for the oligonucleotide length. For low flow rates through the system, the higher cycling frequencies of short strands lead to higher numbers of temperature cycles before a strands leave the system. In the intermediate velocity range, long strands benefit from their significantly higher abundance time, allowing them to cycle more often than the short ones.



**Supplementary Fig. S11 | Quantification of native polyacrylamide gel data from the selection and replication experiment presented in Fig. 4 b, d.** **a**, Raw gel image and selection of the region of interest. **b**, Outliers which are due to residual dust grains are visible due to the long exposure time. They were removed before further analysis. **c**, Removed outliers. **d**, Quantitative data of all 10 gel lanes. The integrated intensities of the 36mer (red, left) and 75mer DNA (blue, right) were evaluated as indicated. The error bars in Fig. 3d and 4d were calculated from the contribution of noise at the end points of the local baselines to the integrated intensities.



**Supplementary Fig. S12 | Quantification of native polyacrylamide gel data from the serial dilution experiment presented in Fig. 4d.** **a**, Size reference: equidistant 200 bp dsDNA ladder. **b**, Raw gel image and selection of the region of interest. **c**, Integrated intensities from panel **d**, of all 8 gel lanes. **d**, Region of interest for quantitative analysis. Outliers were removed before quantification. **e**, Outliers removed from panel **d**.

## Supplementary Videos

### 1) nchem.2155-s2.mp4

#### Supplementary Video 1

Qualitative visualisation of cyclic trajectories inside a 100  $\mu\text{m}$  thick and 2000  $\mu\text{m}$  high rectangular capillary by fluorescent tracer particles, observed through the heated glass wall. A gentle flow perpendicular to the planes of cycling was applied to aid visualisation of the cycling trajectories, gravity pointing downwards. Total length of the video: 15 minutes.

### 2) nchem.2155-s3.mp4

#### Supplementary Video 2

Accumulation of DNA in an electrically heated capillary. The capillary was filled with 0.5  $\mu\text{g}/\text{ml}$  weight-equalised double stranded DNA ladder with 10 equidistant bands from 100 bp to 1000 bp in combination with 0.5 $\times$  SYBR Green I. The capillary was heated through a transparent semiconductor layer. A temperature gradient ranging from 22  $^{\circ}\text{C}$  to 88  $^{\circ}\text{C}$  was applied at the outer walls of the capillary, resulting in a temperature difference from 38  $^{\circ}\text{C}$  to 71  $^{\circ}\text{C}$  inside the capillary. Inner dimensions of the capillary were 100  $\mu\text{m}\times$ 2000  $\mu\text{m}$ . The video was recorded over a time frame of 300 seconds.

### 3) nchem.2155-s4.mp4

#### Supplementary Video 3

Length selective trapping. A capillary with dimensions of 70  $\mu\text{m}\times$ 1400  $\mu\text{m}$  was filled with FAM labelled 75mer and a Cy5 labelled 25mer DNA. An alternating excitation of both dyes was used to separately record changes in molecular concentration. In order to perform selective pressure on trapped molecules, an external inflow of diluted DNA is applied and gradually increased from 2  $\mu\text{m}/\text{s}$  to 6  $\mu\text{m}/\text{s}$ . Below 4  $\mu\text{m}/\text{s}$ , both strands accumulate. In the region between 4  $\mu\text{m}/\text{s}$  and 5  $\mu\text{m}/\text{s}$ , the 75mer DNA withstands the inflow whereas the 36mer DNA is diluted by the external inflow. Total recording time: 5.2 hours.

**4) nchem.2155-s5.mp4****Supplementary Video 4**

Exponential replication of 80mer double-stranded DNA inside a rectangular glass capillary of 100  $\mu\text{m}$   $\times$  2000  $\mu\text{m}$  cross-sectional dimensions visualised by SYBR Green I fluorescence. View through heated side of the capillary, gravity pointing downwards.

Total length of the video: 18 minutes.

## Supplementary References

1. Minami, T., Sonohara, H., Kakumu, T., & Takata, S. Physics of very thin ITO conducting films with high transparency prepared by DC magnetron sputtering. *Thin Solid Films* **270**, 37–42 (1995).
2. Gupta, V. & Mansingh, A. Influence of postdeposition annealing on the structural and optical properties of sputtered zinc oxide film. *J. Appl. Phys.* **80**, 1063–1073 (1996).
3. Davidse, P. D. Theory and practice of RF sputtering. *Vacuum* **17**, 139–145 (1967).
4. Ziegler, J. G., Nichols, N. B. Optimum settings for automatic controllers. *trans. ASME* **64** (1942).
5. Maniatis, T., Jeffrey, A. & Van deSande, H. Chain length determination of small double- and single-stranded DNA molecules by polyacrylamide gel electrophoresis. *Biochemistry* **14**, 3787–3794 (1975).
6. Schneider, C. A., Rasband, W. S. & Eliceiri, K. W. NIH Image to ImageJ: 25 years of image analysis. *Nature Methods* **9**, 671–675 (2012).
7. Reichl, M., Herzog, M., Götz, A. & Braun, D. Why charged molecules move across a temperature gradient: The Role of Electric Fields. *Phys. Rev. Lett.* **112**, 198101 (2014).
8. Reineck, P., Wienken, C. J. & Braun, D. Thermophoresis of single stranded DNA. *Electrophoresis* **31**, 279–286 (2010).
9. Stellwagen, E., Lu, Y. & Stellwagen, N. C. Unified description of electrophoresis and diffusion for DNA and other polyions. *Biochemistry* **42**, 11745–11750 (2003).